Collimator challenges at SuperKEKB and their countermeasures using nonlinear collimator

Shinji Terui,[*] Yoshihiro Funakoshi,[†] Takuya Ishibashi, Haruyo Koiso, Mika Masuzawa, Yu Morikawa, Akio Morita, Shu Nakamura, Hiroyuki Nakayama, Yukiyoshi Ohnishi, Kazuhito Ohmi, Kyo Shibata, Mitsuru Shirai, Yusuke Suetsugu, Makoto Tobiyama, Ryuichi Ueki, and Demin Zhou

High Energy Accelerator Research Organization (KEK), Tsukuba, Japan

Katsunobu Oide

University of Geneva, Geneva, Switzerland

Andrii Natochii

Brookhaven National Laboratory, New York, USA

(Received 27 February 2024; accepted 10 July 2024; published 14 August 2024)

In SuperKEKB, movable collimators reduce the beam background noise in the Belle II particle detector and protect crucial machine components, such as final focusing superconducting quadrupole magnets (QCS), from abnormal beam losses. The challenges related to the collimator, which were not properly considered at the time of SuperKEKB design, have surfaced through experience with its operation. In this paper, we report the collimator operation strategy in SuperKEKB. In addition, a significant challenge of beam collimation due to the future increase in the beam background is highlighted. We also discuss another issue caused by unexpected and sudden beam losses in the machine that damage collimators, leading to weaker beam collimation performance and an increase in transverse impedance. Furthermore, we introduce a novel collimation approach called the nonlinear collimator (NLC) to address these challenges. We detail the concept of NLC and evaluate their effectiveness by assessing the collimator impedance, beam background reduction, and impact on the dynamic aperture. The possibility of using NLCs as absorber collimators to counteract events that damage the collimator is also shown to be helpful.

DOI: 10.1103/PhysRevAccelBeams.27.081001

I. INTRODUCTION

SuperKEKB is an electron-positron collider that achieves a luminosity far exceeding that of its predecessor, KEKB, for exploring new physics beyond the Standard Model [1]. Its main ring (MR) consists of a 7 GeV electron ring (high-energy ring: HER) and a 4 GeV positron ring (low-energy ring: LER) [2]. The design parameters and the values achieved on the last day of the 2022ab run (February 21 to June 22, 2022) at SuperKEKB are shown in Table I.

Thus far, the minimum vertical beta (β) function at the interaction point (IP) (i.e., β_y^*) achieved in SuperKEKB is 0.8 mm, which is the smallest in the world for a production-type accelerator.[1] Since it was challenging to store high current beams at $\beta_y^* = 0.8$ mm, currently $\beta_y^* = 1$ mm is used in the production operation.

SuperKEKB surpasses the luminosity record of KEKB and continues to break the world's highest luminosity value every year. However, achieving a luminosity more than ten times higher for future operations is necessary. To achieve this goal, SuperKEKB requires further squeezing of the vertical beam size at the IP using final focusing superconducting quadrupole magnets (QCS) [3] and storage of higher beam currents, as shown in Table I. In this process, one of the critical issues is the increase in the beam-induced background (BG) in particle detectors [4], which leads to a degradation of the energy and momentum resolutions of the particle detectors and consequently reduces their detection efficiency. To mitigate the BGs, collimators were installed in SuperKEKB to ensure the stable and safe operation of

[*]Contact author: sterui@mail.kek.jp
[†]Contact author: yoshihiro.funakoshi@kek.jp

Published by the American Physical Society under the terms of the Creative Commons Attribution 4.0 International license. Further distribution of this work must maintain attribution to the author(s) and the published article's title, journal citation, and DOI.

[1]An accelerator that delivers beams to physics experiments.

TABLE I. Design parameters and the parameters reached on the last day of the 2022ab run at SuperKEKB.

Parameters	Units	Design LER	Design HER	2022ab run last day LER	2022ab run last day HER
Beam currents	A	3.6	2.6	1.46	1.14
Energy	GeV	4.0	7.0	4.0	7.0
Number of bunches		2500		2249	
Bunch current	mA	1.44	1.04	0.65	0.507
β_x^*/β_y^*	mm	32/0.27	25/0.30	80/1.00	60/1.00
Luminosity	$cm^2\,s^{-1}$	8×10^{35}		4.65×10^{34}	

Belle II [5,6]. Another major issue requiring collimators is the phenomenon, which caused by some unknown reason, of beam hit and damage to the collimators. Damaged collimators were observed to have a reduced BG reduction capacity and increased impedance.

In this paper, we document the challenges in the current SuperKEKB collimators and present a novel nonlinear collimator (NLC) design to address these challenges. An overview of collimator configurations and operational strategy for the current collimation system in SuperKEKB is presented in Sec. II. Challenges related to SuperKEKB collimators in machine operation are described Sec. III. The proposed NLC and its implementation in SuperKEKB LER are detailed in Sec. IV. The advantages of installing a NLC in SuperKEKB and possible risks from it are discussed in Secs. V and VI, respectively. Finally, we summarize our findings in Sec. VII.

II. SUPERKEKB COLLIMATORS

A. Collimation system overview

SuperKEKB has two types of collimators installed: horizontal and vertical collimators. Figure 1 presents a map of the collimators installed around the LER and HER. In this figure, the IR refers to the interaction region. Investigations have shown that in the SuperKEKB MR, vertical collimators are the dominant sources of inductive impedance [7] due to their extremely small gaps. There is a risk of reaching a threshold current of the so-called transverse mode coupling instability (TMCI), which is formulated as follows (see Sec. 2.4.10 of [8]):

$$Ib_{\mathrm{TMCI}} = \frac{C_1 f_s E/e}{\sum k_{\perp,i}\beta_{y,i}}. \tag{1}$$

Here, $C_1 = 8$ denotes a constant value, f_s represents the synchrotron frequency ($f_s = 2.13$ kHz for SuperKEKB LER), and E is the beam energy. The symbols $k_{\perp,i}$ and $\beta_{y,i}$ indicate the vertical kick factor and the beta function, respectively, at the i'th impedance source along the ring. In this paper, the sum of the products of the vertical kick factor ($k_{\perp,i}$) and the local vertical β function ($\beta_{y,i}$) over all the vertical collimators is denoted by $\sum k_{\perp,i}\beta_{y,i}$. In the case of a head length of 10 mm, the kick factor of a SuperKEKB-type vertical collimator is roughly proportional to the half-gap[2] to the -1.5 power. In SuperKEKB operation, we need to find a compromise between two criteria—impedance and beam BG reduction—and determine the collimator gap. Therefore, Eq. (1) serves as one of the main criteria for optimizing the collimator settings for SuperKEKB during operation [9]. Owing to its lower beam energy, the LER beam is more susceptible to impedance effects, necessitating stricter control of the impedance budget. This explains why the LER has fewer vertical collimators than the HER, as shown in Fig. 1. From the perspective of beam instability, the importance of any single vertical collimator in the LER is greater than in the HER. Based on operational experience over the last few years, the D02V1 collimator, positioned as the vertical collimator closest to the IR in the LER, was determined to be the most crucial collimation component. After this collimator was damaged, the BG in Belle II increased significantly and it was difficult to continue the physics run. Details of the damage to the collimator will be described in Sec. III. From this point onward, we will mainly discuss the LER, where the problems associated with collimators are currently more severe.

Figure 2 shows cross-sectional views of (a) a SuperKEKB-type horizontal collimator and (b) a vertical collimator, where two jaws are assembled within one vacuum chamber opposite to each other [5]. For horizontal collimators, the configuration with jaws on both sides of the beam has the disadvantage that the jaws on the outer jaws are irradiated with synchrotron radiation (SR). However, the advantage is that the number of collimators installed can be halved, reducing the total amount of beam coupling impedance. Each collimator jaw is controlled by a motor inside the bellows. The collimator jaw is designed to be replaceable without replacing the collimator chamber when only the jaw is damaged. The disk shown in Fig. 2(b) is a rotating mechanism designed to rotate the vertical collimator chamber to facilitate the replacement of the lower jaw, avoiding interference with the ground.

[2]Distances between the center of the beam orbit and a tip of the collimator jaw.

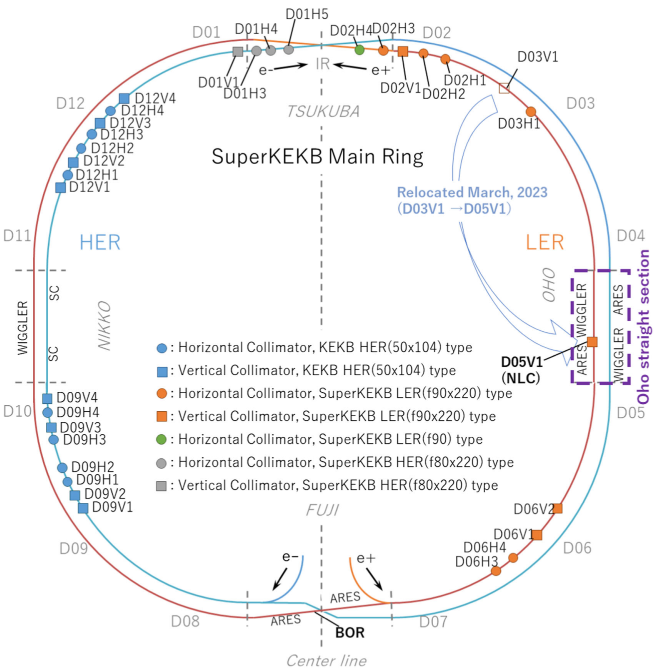

FIG. 1. Location of collimators in MR. Terms H and V in collimator names represent horizontal and vertical collimators, respectively.

Figure 3 shows the fabricated jaw and its dimensions for SuperKEKB-type collimators. The body of the collimator jaw is made of copper, which has good thermal conductivity and machinability. Because the jaws of the horizontal collimators are irradiated by high-density SR, a cooling-water system is included to avoid high temperatures. Tantalum was selected as the material for the collimator head (see the black part attached to the brown copper as shown in Fig. 3). This material has a high melting point, making it difficult to melt when a beam accidentally hits it. Meanwhile, it has a short radiation length because of its relatively high atomic number ($Z = 73$, i.e., high-Z), which provides an effective BG reduction even with a short head length. A short length is preferred to reduce the resistive wall impedance of the collimator head. The results of the impedance calculation for the SuperKEKB-type collimator with changes in head length are presented in Ref. [10].

Collimators contribute to more than 90% of the transverse impedance in SuperKEKB, making it crucial to control their impedance [7]. The transverse impedance causes a transverse kick to the beam and drives TMCI, which must be avoided because it results in a series of beam phenomena harmful to machine operation, such as beam size blowup, beam loss, and consequent damage to critical components.

The vertical beam size is strongly squeezed at the IP to increase the luminosity in SuperKEKB. Consequently, the vertical β function in the QCS ($\beta_{y,\mathrm{QCS}}$) is much larger than that elsewhere. In contrast, the inner diameter of the QCS beam pipe (R_{QCS}) in SuperKEKB ($R_{\mathrm{QCS}} \sim 27$ mm in the smallest vertical section [11]) is small, because the QCS magnets are designed to require high magnetic field gradients to squeeze the beam at the IP. These factors determine that, from the BG point of view, the beam losses

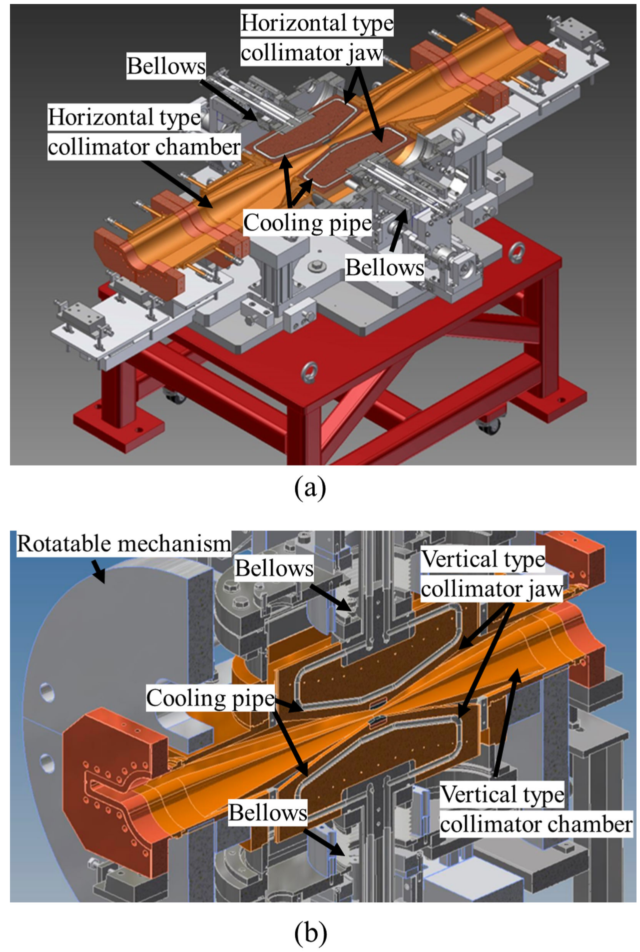

FIG. 2. Schematic drawing of the cross section of (a) a SuperKEKB-type horizontal collimator and (b) a SuperKEKB-type vertical collimator.

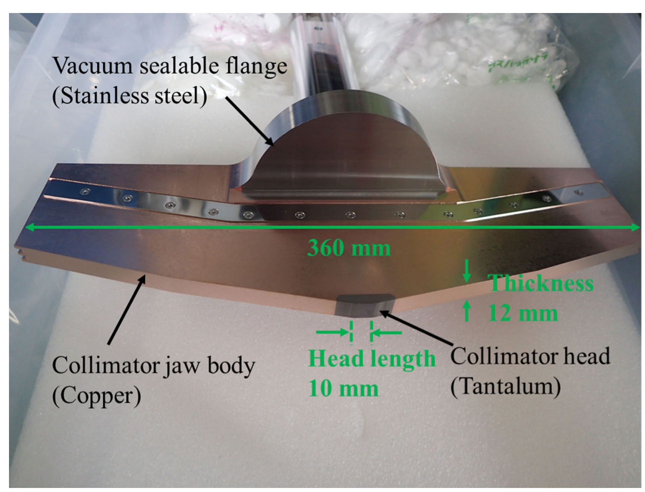

FIG. 3. Photo of the SuperKEKB-type collimator jaw.

near the QCS beam pipe set a bottleneck of the whole ring. To reduce beam losses in the QCS beam pipe, the half-gap of the vertical collimators scales solely as $R_{\rm QCS}\sqrt{\beta_{y,i}/\beta_{y,\rm QCS}}$ [9] and becomes quite narrow (e.g., 1–3 mm for critical vertical collimators). The position of the beam center of mass within the collimator chamber is determined through measurements using beam position monitors both upstream and downstream of the collimator. Alignment of the collimator jaws is also adjusted using the beam [12].

B. Beam background sources

The major sources of beam background at SuperKEKB are described below. Touschek scattering effect involves intrabunch interactions, leading to energy gain and loss among particles within the same bunch. This phenomenon induces horizontal oscillations when an energy change occurs in a dispersive region. Horizontal collimators installed in the arc sections play a crucial role in effectively mitigating beam loss near the detector. Beam-gas Coulomb scattering occurs when beam particles interact with residual gas molecules in the beam pipe, resulting in transverse oscillations. The most troublesome beam loss occurs at the QCS due to vertical oscillation. Consequently, vertical collimators with small jaw openings are essential for protecting the QCS and the surrounding Belle II detectors. These single-beam BG sources dominated the early stages of SuperKEKB commissioning.

In addition to single-beam effects, the collision of the two beams introduces luminosity BG. In the Radiative Bhabha process, beam particles lose energy through gamma emission and are over-bent by the Belle-II solenoid field due to the nonzero crossing angle with the solenoid axis. These beam particles are lost upon hitting the downstream beam pipes immediately after the interaction point. Therefore, collimation has limited efficacy in mitigating this type of beam BG. As SuperKEKB luminosity improves, the contribution of luminosity BG becomes more pronounced, approaching comparability with single-beam BGs. When we achieve the target luminosity of SuperKEKB, luminosity BG is anticipated to dominate.

More detailed description of beam BG sources at SuperKEKB can be found in [13].

C. Operational strategy

From the viewpoint of tuning using the vertical collimators and their control, it is better to install the collimator at a location where the β function is larger. On the other hand, the instability (TMCI) driving term is proportional to $\sum k_{\perp,i}\beta_{y,i}$ as is shown in Eq. (1). In general, a smaller collimator gap is required at a smaller $\beta_{y,i}$ section to keep an equivalent collimation capability. This implies that a smaller $\beta_{y,i}$ results in a higher $k_{\perp,i}$. Nevertheless, the product $k_{\perp,i}\beta_{y,i}$ can become smaller with a smaller $\beta_{y,i}$ [9]. The collimator locations and their actual use were chosen based on the above considerations to satisfy the conditions for both TMCI and BG reduction [6,9].

During operation from 2020 to 2022, four vertical collimators were used in the LER: D06V1, D06V2, D03V1, and D02V1. Among them, the vertical betatron phase advance between D06V1 and D02V1 is close to an integer number of 2π. The vertical betatron phase advance between D02V1 and QC1RP, which is the final focusing quadrupole located upstream of the IP, was chosen to be approximately π to reduce beam loss at the quadrupole. D06V1, depicted as the vertical collimator closest to the injection point in Fig. 1), has its aperture narrowed as much as possible without affecting the injection efficiency.[3] Its role is to cut the tail of the stored beam and stop the abnormally injected beams at the location as far away from the IR as possible. We refer to D06V1 with a narrow aperture as the primary collimator. We refer to collimator that actively narrow the half-gap and set the ring aperture as narrow as possible without adversely affecting injection efficiency as primary collimator. The intention is for the primary collimator to intercept the beam first in case it deviates along an abnormal orbit. D02V1, being the most critical collimator for protecting the Belle II detectors, is used with extra caution to avoid damage, as previously mentioned. D06V2 collimates the halo of the stored beam that cannot be collimated by D06V1, while serving as a backup collimator for abnormally injected beams in case the D06V1 is damaged. D03V1 was initially installed for further BG reduction, although it is currently seldom used due to the significant increase in transverse impedance if D03V1 is also activated.

During machine operation, based on these findings, the $\sum k_{\perp,i}\beta_{y,i}$ value is controlled and the half-gap is adjusted to suit the injection efficiency, beam lifetime, and BG conditions.

III. CHALLENGES RELATED TO SUPERKEKB COLLIMATORS

A. Background reduction for future operation of Belle II

One of the key challenges for collimation is effectively handling the expected significant increase in beam BG during the future operation of Belle II. Among the subdetectors in Belle II, the time-of-propagation (TOP) counter is most vulnerable to beam BG. The degradation of photocathode of microchannel plate-photomultiplier tubes (MCP- PMTs) used in the TOP counter determines the upper limit of the beam BG, as discussed in [6,14].

Figure 4 illustrates the TOP beam BG during recent operations as a function of the stored beam current in the LER. The LER beam current is represented on the

[3]The ratio is between the stored charge after injection and the injected charge.

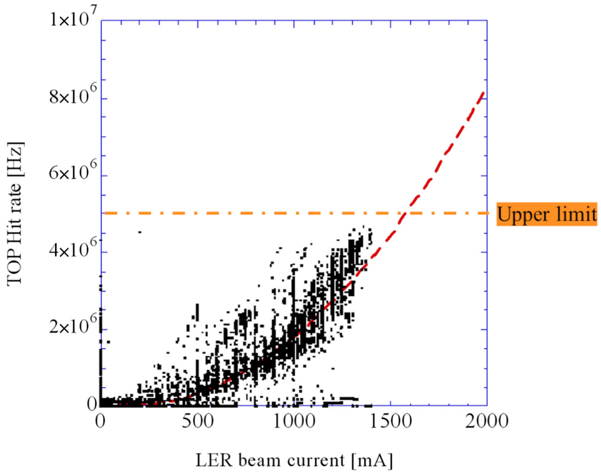

FIG. 4. Measured BG in the TOP MCP-PMTs (black markers). Red, dashed and orange, dot-dashed lines represent extrapolated TOP BGs based on measurements and detector limit, respectively.

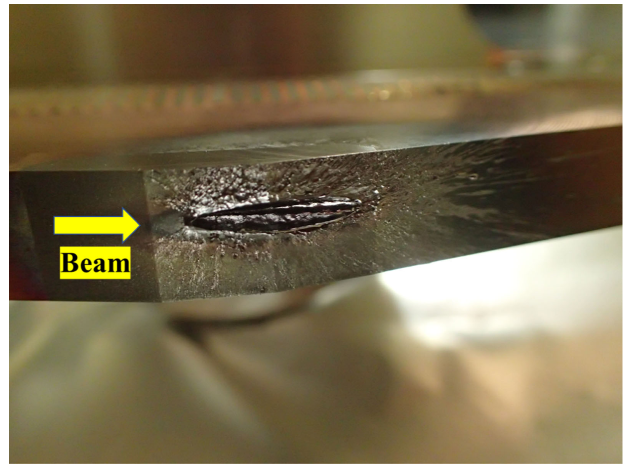

FIG. 5. Collimator jaw with a scar on the surface of the collimator head due to the passage of the abnormal beam.

horizontal axis, and the BG is predominantly influenced by the LER contribution. However, due to the BG of collision conditions, the HER contribution is also present. Depending on the operating conditions, the beam current of the HER was approximately equal to the LER beam current times 0.8.

With the current beam current achieved thus far, the TOP BG remains below the limit determined by the lifetime of MCP-PMT photocathodes. Therefore, the beam BG is not a bottleneck for high-luminosity endeavour. However, without further mitigation, the TOP background is expected to exceed the limit as the beam current is increased for higher luminosity.

Furthermore, when β_y^* is reduced from 1 mm to smaller values (0.8 mm, 0.5 mm, etc.), aimed at higher luminosity, β_y inside the QCS becomes larger, and therefore, we set even narrower half-gaps in the collimator to achieve effective mitigation of beam loss inside the QCS.

To overcome those challenges, we have decided to install a so-called "nonlinear collimator (NLC)," which provides good beam collimation power but with much less impedance. The details of NLC can be found in Sec. IV.

To address this increase in BGs, it is necessary to use narrower half-gap settings in the collimators. However, narrow half-gap settings reduce beam lifetime and injection efficiency.

B. Collimator damage due to sudden beam losses

Another significant challenge related to collimators is the damage to vertical collimator jaws caused by abnormal beam impacts. Such damages have occurred approximately 15 times thus far, and their mechanisms are still under investigation. Intuitively, the vertical collimators with the smallest gaps in the ring, which are set to protect other key components, are the first to be hit by abnormally unstable beams. Only vertical collimators are damaged because horizontal collimators have a wider half-gap than vertical collimators due to the injected beam oscillations. The horizontal collimator was damaged during the accidental fire of the injection kicker; however, this event is not presented in this paper because the cause is clear.

Figure 5 shows an example of the collimator head damaged by the abnormal beam. Straight scratches were observed on the head surface through which the beam passed. This area melted due to a rapid increase in temperature caused by very fast (on the scale of a few tens of microseconds) and dense energy deposition from the impinging beam [15]. BG levels before and after the damage event are shown in Fig. 6 with the particle hit rate observed by the TOP counter and the beam current on the

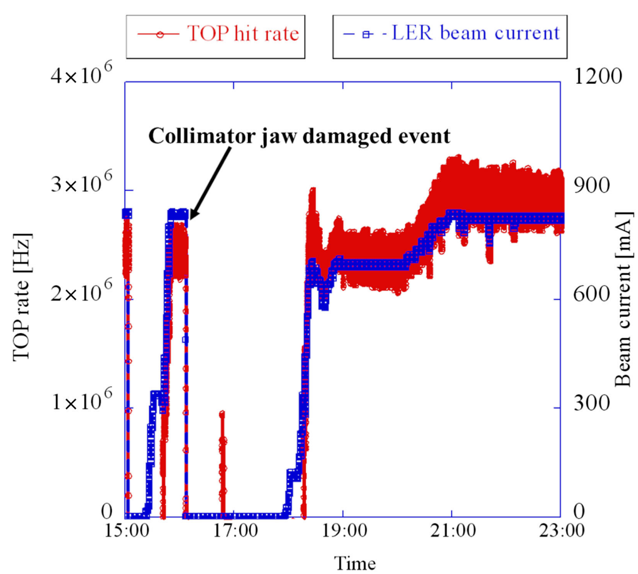

FIG. 6. TOP BG hit rate and beam current before and after the collimator jaw damaged event.

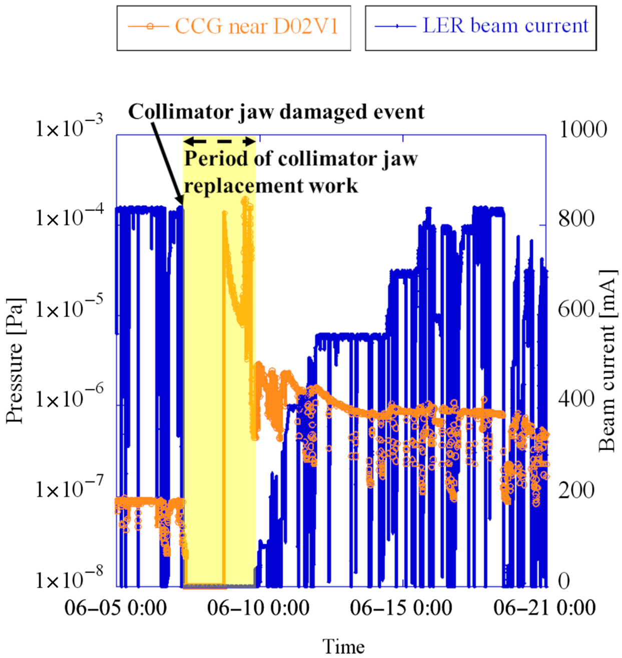

FIG. 7. Vacuum pressure and beam current before and after the collimator jaw replacement work.

vertical axes. It can be observed that the BGs increased after the collimator damage at the same stored beam currents. After this event, additional beam losses and consequently high BGs caused the Belle II detector to trigger frequent beam aborts. Consequently, accelerator operation had to be interrupted to replace the damaged collimator jaw to recover a stable operation. As a side effect, the vacuum pressure near the damaged collimator changed before and after jaw replacement, as depicted in Fig. 7, where the horizontal axis represents time and the vertical axes represent the pressure and beam current, respectively. The pressure values were measured using a cold cathode gauge close to the air-exposed collimator. After exposure to air, it took quite a long time for the vacuum pressure near the damaged collimator to decay to the level before the damage event. In the case of Fig. 7, the pressure did not reach the value before jaw replacement, even after more than ten days of beam operation. In conclusion, such beam loss events have a significant impact, not only in terms of lost operating time but also because of pressure deterioration after jaw replacement.

The phenomenon of collimator damage occurs with a large amount of beam loss in approximately three turns (i.e., approximately 30 μs) of the beam circulation. However, no clear signs of conventional beam instabilities, which should occur with dipole beam oscillations and with a growth time much longer than three turns, were observed before the beam was aborted. Hence, we refer to this sudden beam loss (SBL) phenomenon to distinguish it from classical beam instabilities. To the best of our knowledge, no similar phenomenon has been observed in other circular e^+e^- colliders. Events of SBL often occur during collision conditions, however, they can also occur when the opposite beam current is very low. Therefore, it is presumed that the cause of the SBL is not related to the beam-beam effect. In SuperKEKB, SBLs occur at currents higher than 500 mA. However, empirical experience showed that the risk of collimator damage increased when the bunch current exceeds 0.7 mA. Thus, in actual operation, we defined a policy of increasing the luminosity by increasing the number of bunches, but keeping the bunch current below 0.7 mA. However, as shown in Table I, the number of bunches almost reaches the upper limit of 2346 in the 2022ab run. To achieve an even higher luminosity, there is no other way than to increase the bunch current and squeeze β_y^* further. Therefore, the limited bunch current is a major challenge for SuperKEKB.

Figure 8 presents data collected using a bunch oscillation recorder (BOR) [16] during collimator damage, specifically four turns before and one turn after the beam-aborted time stamp. Positioned near the injection point in the LER, as depicted in Fig. 1, vertical positions (units: mm) and current losses (units: mA) as a function of the bucket number along the bunch trains (with two gaps to create enough rising time for the beam abort system) in five turns are shown in Fig. 8. Positioned near the injection point in the LER, as depicted in Fig. 1, the BOR records vertical positions (in mm) and current losses (in mA) plotted against the bucket number along the bunch trains, with two gaps allowing for sufficient rising time for the beam abort system, spanning five turns (as shown in Fig. 8). The region outlined by the red dashed line highlights the time at which the vertical beam position begins deviating from the stable orbit, albeit without any observed beam loss. Subsequently, in the following turn, beam losses started occurring in the bunches with significant vertical displacements, denoted by the orange dashed line within the time window. This observation illustrates a correlation between beam losses and the vertical positions of the bunches. It is important to note that the BOR only measures the center of mass of the bunches in the transverse plane. Therefore, while this correlation suggests a link between vertical positions and beam losses, it does not definitively rule out the possibility of beam losses resulting from transverse beam size blowups. In the future, SuperKEKB plans to install and test a device capable of monitoring the beam size in a bunch-by-bunch (B × B) regime. Further details on SBLs can be found in Ref. [17].

C. Vertical beam instability

In the SuperKEKB LER, instances of vertical beam size blowup were observed at specific bunch currents due to the interplay between impedance effects and the B × B feedback system, as detailed in Refs. [18,19]. Figure 9 illustrates the outcomes of the fast Fourier transform (FFT) analysis conducted on data acquired using the BOR during

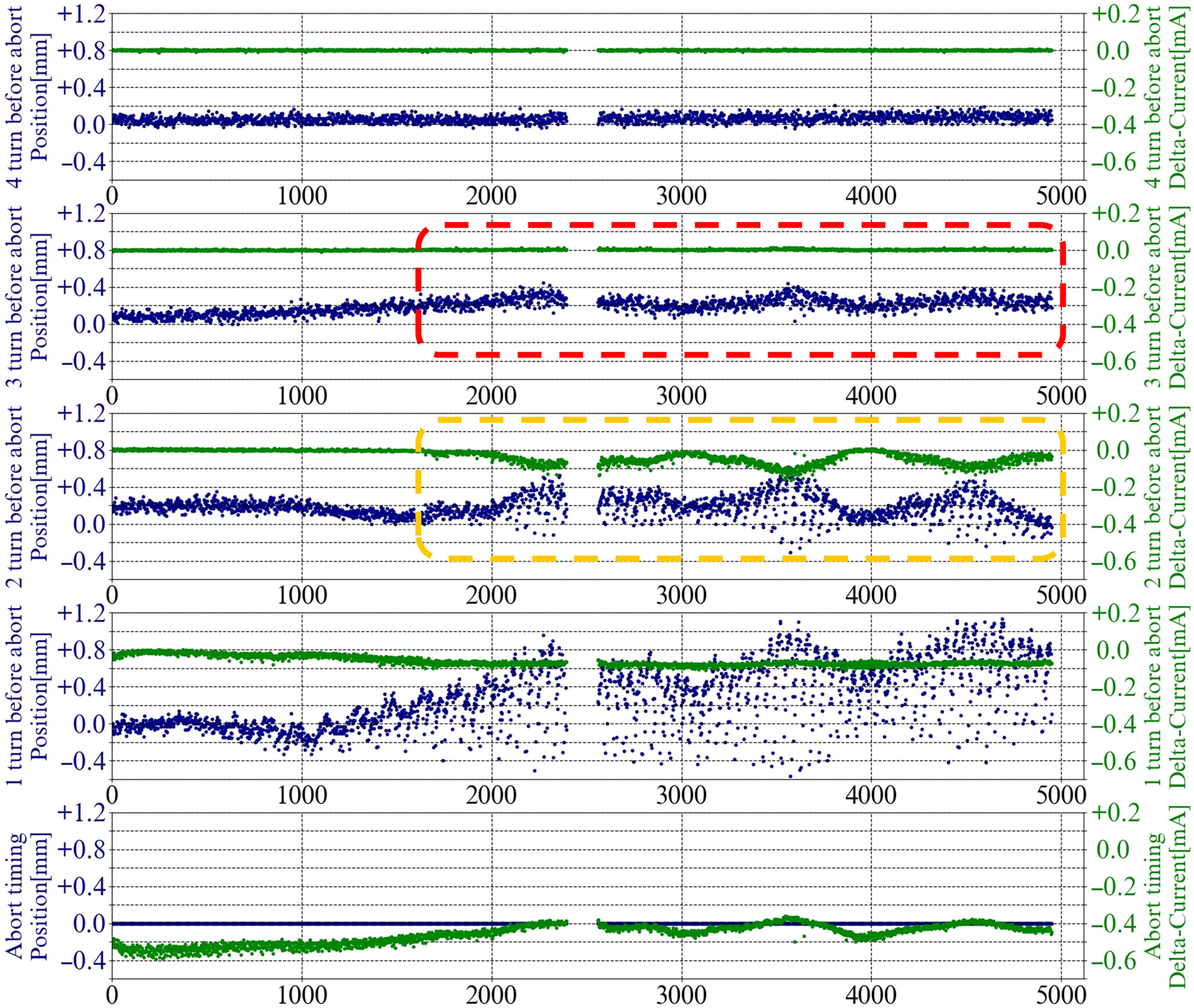

FIG. 8. Vertical positions (blue dots) and lost currents (green dots) of the bunches along the bunch trains in the last five turns during the collimator damage event. Each subfigure corresponds to one turn and there are two gaps between the bunch trains.

periods of vertical beam size blowup. A pilot bunch, which does not collide with the opposite beam, is intentionally excited to measure the coherent betatron tune (0 mode indicated as ν_y). The result of the FFT analysis of the pilot bunch is shown in Fig. 9(b). The 0 mode tune shifts to the left side with increase of the bunch current; this is a well-known phenomenon of impedance effects. The same analysis is also performed for nonpilot bunches, as shown in Fig. 9(a). The measurements were performed under single-beam conditions and with as few as 33 bunches to avoid the effects of multibunch instability.

Comparing Figs. 9(a) and 9(b), it is evident that the oscillations of the nonpilot bunches were not at the 0 mode frequency of ν_y, but at a frequency near $\nu_{y0} - \nu_s$ with ν_{y0} the nominal fractional betatron tune at zero current. This frequency is designated as the–1 mode. The 0 and–1 modes are simultaneously seen in the pilot bunch, but they have not yet merge for all bunch currents shown in Fig. 9(b). This suggests that the TMCI threshold should be higher than 0.94 mA (the maximum bunch current for this measurement), and the vertical blowup that appears with the observable $\nu_{y0} - \nu_s$ is not attributed to TMCI. When the $B \times B$ feedback system was turned-off, the vertical beam size blowup was not observed even at high bunch currents where the vertical beam size blowup was observed when the $B \times B$ feedback system was turned-on. Therefore, we call it the "−1 mode instability" to make it different from TMCI. The previous one is excited by the feedback system in the presence of impedance effects, and the latter one is a pure impedance effect.

To assess the impact of the collimator condition on the "−1 mode instability," we compared the vertical emittance measurements obtained from x-ray monitors [20] before and after collimator damage. These measurements were

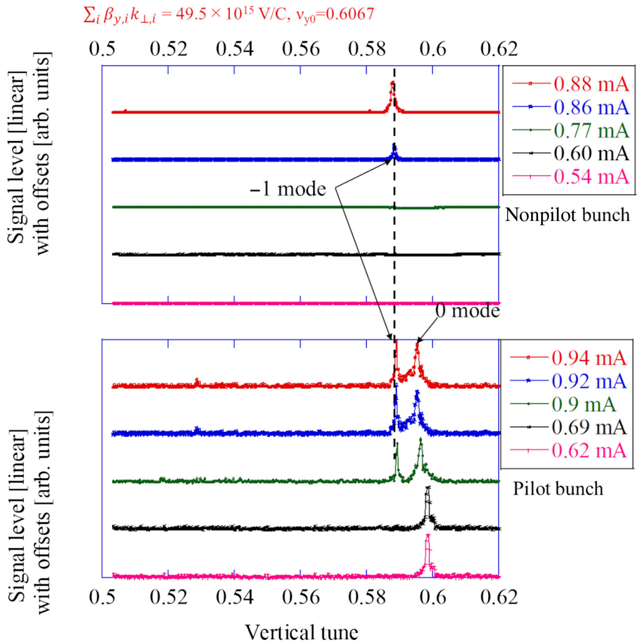

FIG. 9. Results of the FFT analysis of vertical beam motion data collected using the LER BOR.

conducted in a single-beam mode, excluding beam-beam effects, with a reduced number of bunches (93) compared to the harmonic number (5120) to exclude multibunch effects. The results, depicted in Fig. 10, illustrate the bunch

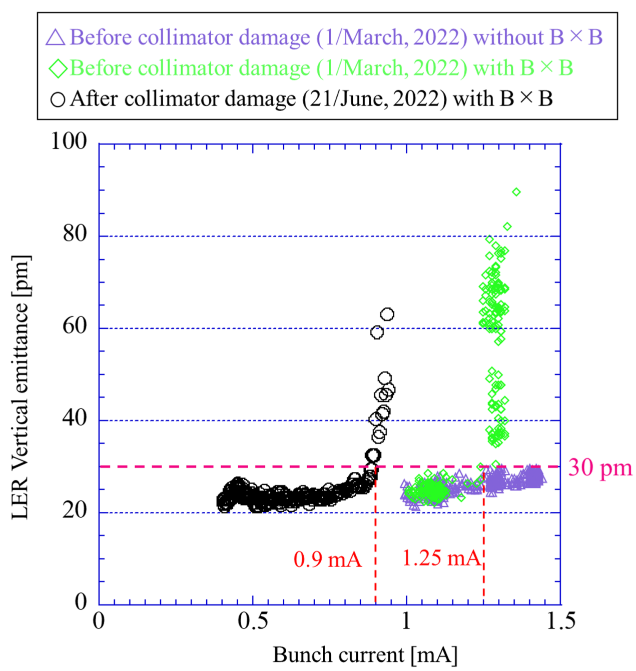

FIG. 10. Vertical beam emittance versus bunch current with $\beta_y^* = 1$ mm, before (green diamonds) and after (black circles) the event of collimator jaw damage with B × B feedback on. The data of purple triangles show the measurement with B × B feedback off.

current on the horizontal axis and the emittance on the vertical axis. Green and black points represent measurements before and after collimator damage, respectively, with B × B feedback turned-on, while purple dots denote measurements before collimator damage with B × B feedback turned-off. Typically, the vertical emittance in LER ranges from approximately 30–45 pm during a physics run, considering beam effects and other collective phenomena. For this study, a vertical emittance of 30 pm was set to identify the threshold current for vertical blowup. It is evident that before and after the damage event, the threshold current was approximately 1.25 and 0.9 mA, respectively, with B × B feedback. However, without B × B feedback, the threshold was not observed below 1.4 mA. This indicates that the B × B feedback excites the "–1 mode instability."

It is notable that the half-gap setting remained almost unchanged before and after the damage, with corresponding β-weighted kick factors being similar: $\sum k_{\perp,i}\beta_{\mathrm{y},i} = 33.5 \times 10^{15}$ V/C before damage and $\sum k_{\perp,i}\beta_{\mathrm{y},i} = 35.6 \times 10^{15}$ V/C after damage, as calculated numerically. It is evident that the aforementioned notable decrease in the blowup threshold current cannot be attributed to a change in the half-gap setting but rather to the damaged collimator head. Since the beam-hit jaw has clear protrusions, as shown in Fig. 5, it is fair to conclude that the damaged jaw significantly increases the impedance, causing a decrease in the blowup threshold. Furthermore, with the exclusions of beam-beam and multibunch effects, the vertical blowup can be attributed to a single-bunch instability.

The beam-beam effect can also drive a single-bunch TMCI-like instability and cause vertical blowup through an interaction with vertical impedance, as recently discovered [21].

Another evidence of a large increase in impedance from the damaged collimator is the extra betatron tune shift from the measurement. The results are summarized in Fig. 11 with the vertical tune shift per 1 mA bunch current on the vertical axis and β-weighted kick factor $\sum k_{\perp,i}\beta_{\mathrm{y},i}$ (the values are from numerical calculations with given collimator gap settings) on the horizontal axis. The green dots denote regular vertical tune shifts. After collimator damage, the tune change increased with the same collimator gap settings (as indicated by the same values of $\sum k_{\perp,i}\beta_{\mathrm{y},i}$). We speculate that one reason for the higher impedance is the protruding surface of the collimator head, visible in Fig. 5, which brings it closer to the beam after damage, even though its position remains the same before and after the collimator damaged event.

In conclusion, the investigations revealed that a damaged vertical collimator significantly increased the vertical impedance, thereby significantly reducing the threshold of the vertical beam size blowup and causing additional tune shifts. As shown in Fig. 11, the vertical tune shift at 1 mA after collimator damage is already close to synchrotron tune ν_s,

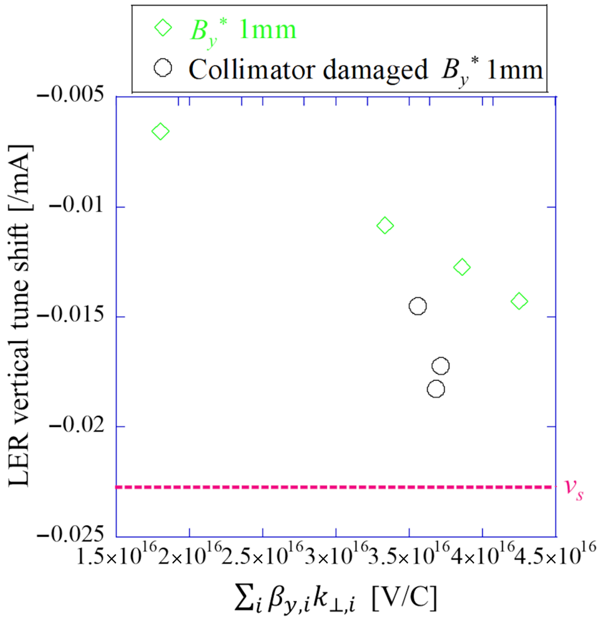

FIG. 11. Vertical tune shift per mA versus bunch current, before (green, open diamonds) and after (black, open circles) the event of collimator jaw damage at $\beta_y^* = 1$ mm.

suggesting that the risk of TMCI increases. Furthermore, a larger impedance would worsen its interplay with the beam-beam through mode coupling [22]. This is another significant challenge for SuperKEKB collimators.

IV. NONLINEAR COLLIMATOR FOR SUPERKEKB

The challenges described in the previous section motivated the installation of an NLC to SuperKEKB LER. The hardware installation in the SuperKEKB tunnel was completed during the long-term shutdown 1 (LS1) from summer 2022 to the end of 2023. In this section, we provide an overview of the NLC and describe the LER lattices with the NLC.

A. Concept of the nonlinear collimator

The concept of NLC was proposed for the future linear collider in the early 1990s [23–26]. For the next linear collider, a scheme using normalsextupole pairs was proposed for betatron collimation in both horizontal and vertical planes simultaneously [23,25]. The motivation of adopting the NLC was to avoid emittance dilution caused by wakefield effects of narrow aperture collimators and also to avoid the damage of the collimators by hits of missteered beams. The NLC was also proposed for LHC in the 2000s [27,28]. Toward the luminosity upgrade of the LHC, a scheme using a pair of skew-sextupoles was proposed for betatron collimation in both horizontal and vertical planes. The main purpose of adopting the NLC was to reduce the collimator-induced impedance that may limit the beam intensity in future LHC. Conceptually, the benefits of adopting NLC in next linear collider and LHC also apply to SuperKEKB. SuperKEKB will be the first actual machine in the world and accelerator history to use NLC. In our scheme, a pair of skew-sextupoles will be used for betatron collimation in the vertical plane. The purpose of the NLC at SuperKEKB is to reduce the collimator-induced impedance in the vertical plane, which is addressed in Sec. III.

B. Lattice design for the nonlinear collimator

Figure 12(a) shows the design lattice around the NLC region. A pair of skew-sextupole magnets with the same

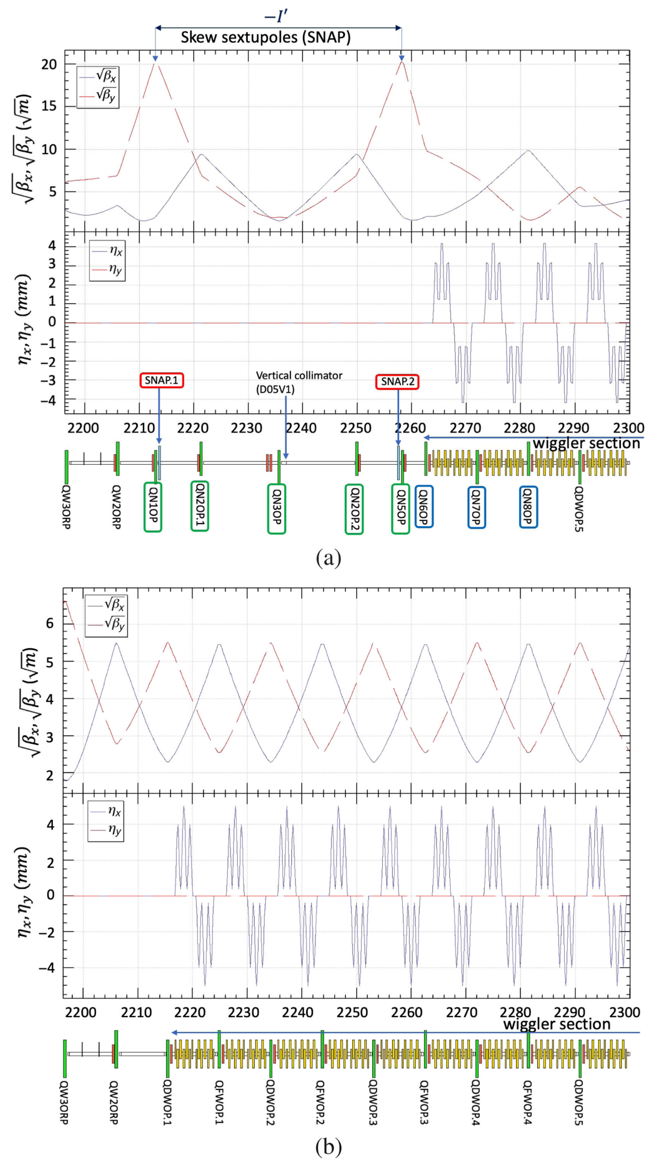

FIG. 12. (a) Layout of the design lattice for the NLC. The horizontal axis is the distance from the IP in meters. (b) Layout of the current machine lattice of the same area as (a).

TABLE II. Design parameters of the NLC at the SuperKEKB LER.

Parameters		Units	Values
β functions at SNAP	$\beta_{x,ys}$	m	7.08/378.5
β functions at D05V1	$\beta_{x,yc}$	m	3.55/4.05
Components of the transfer matrix between SNAP.1 and D05V1	R_{33}/R_{34}	m	3.11/37.2
Phase advance between SNAP.1 and D05V1	$\Delta\nu_{x,y,c}$	2π	0.323/0.301
Phase advance between SNAP.1 and the IP	$\Delta\nu_{x,y,IP}$	2π	11.709/12.750
Strength of SNAP	K_s	m^{-2}	6.00
SNAP bore radius	b_s	mm	56
SNAP effective length	L_s	m	0.335
SNAP pole tip field	B_s	T	0.71

strength named SNAP are connected by a $-I'$ transform to cancel the geometric optical aberrations. Here, the $-I'$ transform is a (4×4) transfer matrix whose diagonal elements are–1 and off-diagonal elements are zero except for the nonzero (2,1) and (4,3) elements. The phase advance between the paired skew-sextupoles is set to π in both planes, and that between the first SNAP (SNAP.1) and the vertical collimator named D05V1 is near $\pi/2$ in both planes. In addition, the vertical phase advance between the SNAPs and the final focus quadrupoles (QC1LE and QC1RE in QCS) are set to $N\pi$, where N is an integer to reduce beam losses in the quadrupoles that are the main source of the detector BG. Moreover, we decided to relocate the D03V1 collimator (see Fig. 1), which was unused in the previous operation due to its high impedance and to use it as the NLC (D05V1).

The kick by a skew-sextupole is expressed with the thin lens approximation as

$$\Delta p_y = \frac{K_s}{2}(y^2 - x^2), \qquad \Delta p_x = K_s xy. \tag{2}$$

Here, Δp_x and Δp_y are the kicks in the horizontal and vertical planes, respectively. The variables x and y are the horizontal and vertical orbit offsets at the skew-sextupole, respectively. The strength of the skew-sextupole (K_s) is defined using the following equation:

$$K_s = \frac{L_s}{B\rho}\frac{\partial^2 B_x}{\partial y^2}. \tag{3}$$

Here, $B\rho$, B_x, and L_s denote the magnetic rigidity, the magnetic field in the horizontal direction, and the effective length of the magnet, respectively. The concept behind NLC is to apply a strong kick to the beam halo particles in the vertical direction at SNAP.1 and then remove them from the beam at the followed vertical collimator (D05V1). To facilitate this collimation, the vertical β functions in the skew-sextupoles are set to a large value. Table II shows details of the design parameters of the NLC. To scrape particles with offsets $|y| > y_s$ at the center of SNAP.1, the collimator (D05V1) half-gap should be set to a certain value (approximately 5.9 mm, details are given below):

$$A_{y,c} = \frac{1}{2}R_{34}K_s y_s^2. \tag{4}$$

The simulated distributions of beam particles impinging on and passing through the NLC in the vertical plane are depicted in Fig. 13. These simulated particles undergo scattering due to the Touschek effect and beam-gas interactions, resulting in the formation of a beam halo. They are tracked through the machine lattice for 1000 turns [6].

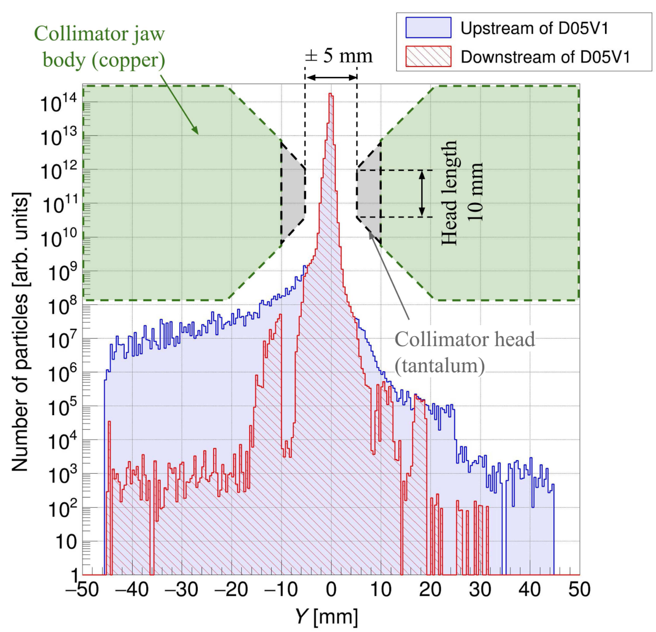

FIG. 13. Simulated distribution of beam halo particles in the vertical plane upstream (blue, solid) and downstream (red, hatched) of the NLC element in the machine lattice file. The two distributions represent the accumulated number of halo particles after 1000 machine revolutions with a bin size of 0.4 mm. These distributions are constructed at the same s location as the NLC is positioned, utilizing the same beam optics functions.

The solid-blue histogram in Fig. 13 illustrates the distribution of beam particles at D05V1 before encountering the collimator downstream of SNAP.1, while the red hatched histogram displays the particle distribution at D05V1 after passing the collimator, upstream of the second SNAP (SNAP.2). It is seen that upstream of the NLC, the halo is asymmetrical rather than Gaussian due to an asymmetrical angular kick of SNAP.1: particles located far from the beam center in both the horizontal x and vertical y directions are kicked in the same vertical direction $\Delta p_{\mathrm{y}} \sim (y^2 - x^2)$. Moreover, there is a depletion of particles with $|y| >$ 5 mm downstream of the collimator, indicating that some impinging particles are absorbed by the collimator materials upon passing through the NLC. The reason why the beam halo distribution in the hatched-red histogram in Fig. 13 is not smooth is due to the different number of particles that can be absorbed due to the different radiation lengths of tantalum and copper.

The baseline scheme for utilizing the NLC involved substituting the primary collimator (D06V1) with D05V1. To illustrate the extent of vertical impedance reduction achievable with this replacement, we compared the apertures of D06V1 and D05V1 to ensure equivalent collimation capability. Table III shows a comparison of the aperture of vertical collimators in the LER on December 20, 2021. The collimator apertures were experimentally determined to minimize the detector BG on condition that the collimator setting does not affect the beam injection efficiency and beam lifetime. This table indicates the acceptance, which represents the collimator aperture normalized by the beam size at each collimator. The vertical beam size (σ_{y}) was computed using the assumed vertical emittance of 43.2 pm, which 1% of the horizontal emittance, and β_{y} at each collimator. Notably, the apertures of key collimators (D06V1 and D02V1) were narrower than the aperture of the QCS beam pipe in the vertical direction. Table III additionally displays the aperture of D05V1, which offers collimation capability equivalent to D06V1, i.e., the $\pm 56.8\sigma_{\mathrm{y}}$ collimation. The collimator aperture of D05V1 is calculated by using Eq. (4) and the $56.8\sigma_{\mathrm{y}}$ aperture of 7.26 mm at SNAP.1. It is important to note that only one side of the collimator jaw, either the top or bottom, depending on the skew-sextupole polarity, provides the necessary collimation, as evident from Eq. (2). Here, $k_{\perp,i}$ of D05V1 is calculated in this table with both jaws set to the same half-gap. A comparison of $k_{\perp,i}\beta_{\mathrm{y},i}$ values between D06V1 and D05V1 reveals that replacing D06V1 with D05V1 can reduce the contribution to the $\sum_i k_{\perp,i}\beta_{\mathrm{y},i}$ value from the collimator by more than 30. Further details on the impedance reduction are elucidated in the following section.

TABLE III. Comparison of the LER collimator apertures as on December 20, 2021.

Collimators (magnet)	β_y (m)	Half-gap (mm)	Half-gap $/\sigma_{\mathrm{y}}$	$k_{\perp,i}\beta_{\mathrm{y},i}$ (10^{15} V/C)
QC1RP	764.0	13.5	74.3	
D02V1	11.9	1.07	47.2	13.4
D06V2	20.6	2.685	90.0	5.8
D06V1	67.3	3.065	56.8	15.6
D05V1	4.05	(+ or −) 5.89	56.8[a]	0.5

[a]Effective collimation capability in units of σ_{y}.

C. Properties of the nonlinear collimator

As shown above, one side of D05V1 jaw provides the vertical collimation. The other side of the jaws can work as the horizontal collimator, according to Eq. (2). Because β_{x} at the center of SNAP.1 is small, 7.08m, the effectiveness of the horizontal collimation is low. Setting the jaw for the horizontal collimation at the same half-gap as the vertical collimation jaw, 5.68 mm, gives only $\sim 31.0\sigma_{\mathrm{x}}$ collimation, while a typical acceptance value of other LER horizontal collimators is about $20\sigma_{\mathrm{x}}$.

The vertical collimation by the nonlinear collimator has some different property from a typical, "linear" collimator due to its nonlinearity. The criterion of the beam collimation is given by Eq. (4). More precisely, the beam collimation condition of the NLC in vertical phase space is expressed as

$$P_{\mathrm{y}} > -\frac{1}{2}K_{\mathrm{s}}y^2 - \frac{R_{33}}{R_{34}}y + \frac{y_{\mathrm{col}}}{R_{34}}. \tag{5}$$

Here, y and P_{y} are particle coordinates at the first SNAP (SNAP.1). R_{33}, R_{34}, and y_{col} (the vertical aperture of D05V1) are given in Tables II and III. In Fig. 14, the parabolic border of the collimation by the NLC expressed by Eq. (5) is depicted. The $\pm 56.8\sigma_{\mathrm{y}}$ aperture of the typical collimator, which is virtually located at SNAP.1, is also depicted in this figure. The hatched areas in the graph show the region in the vertical phase space, where particles are collimated by a conventional collimator but not by the NLC. The beam ellipses which correspond to $56.8\sigma_{\mathrm{y}}$ and $80\sigma_{\mathrm{y}}$ betatron oscillations are also drawn in this figure as examples. In the case of the $80\sigma_{\mathrm{y}}$ oscillation amplitude, for example, only particles in a very small fraction of the betatron phase (shown in red) are collimated by the conventional collimator and not by the NLC. Therefore, the NLC offers collimation capability almost equivalent to that of a typical conventional collimator. However, this estimation needs confirmation through measurements.

D. Lattice modifications for the nonlinear collimator

Figure 12(b) illustrates the current machine lattice of the same area as shown in Fig. 12(a). This is "OHO" straight

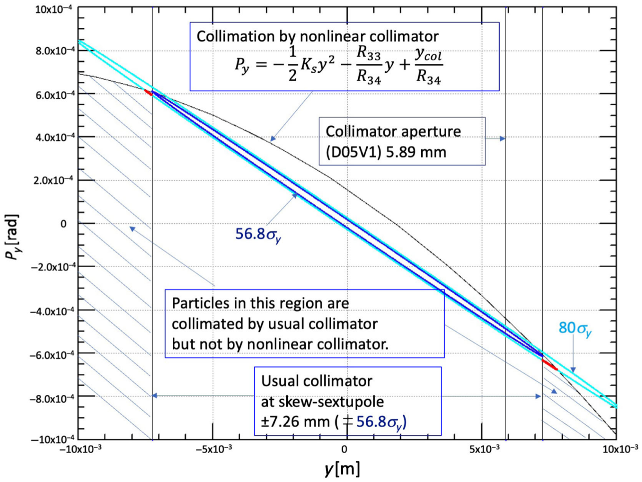

(a)

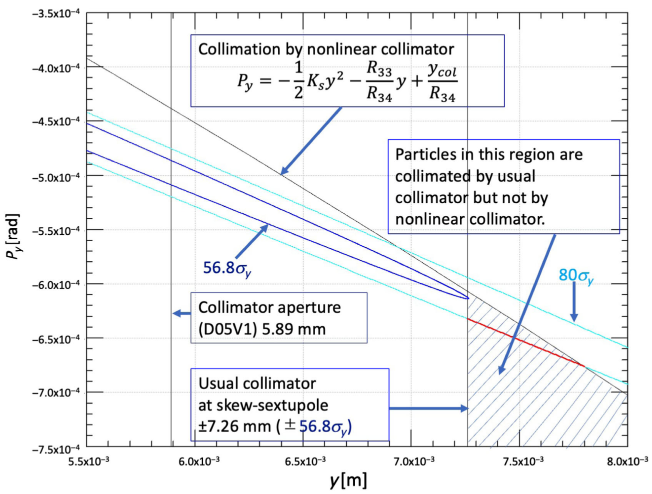

(b)

FIG. 14. (a) Collimation by the NLC in a vertical phase space at the skew-sextupole. (b) Enlarged view of the lower right part of (a).

section, which hosts rf cavities and wiggler magnets. Large-scale modifications of the LER lattice, as illustrated in Fig. 12(a), were implemented during a long shutdown 1 (LS1) between June 2022 and December 2023 to achieve the lattice conditions with nonlinear optics discussed above. These modifications can be summarized as follows: (i) Two skew-sextupole magnets (SNAPs) and a power supply for them are newly constructed. (ii) The wiggler magnets in the NLC region are removed to avoid irradiation of the vertical collimator by SR. (iii) The existing magnets marked in green color in Fig. 12(a) are relocated and powered by independent power supplies. (iv) The existing magnets marked in blue color in Fig. 12(a) remain at the original place, but they are powered by independent power supplies.

As a consequence of removing the wiggler magnets, the radiation damping time in the transverse direction increases from 45.7 to 53.1 ms. The extended radiation damping time could potentially impact beam-beam performance and injection efficiency, a matter to be explored in the subsequent section.

V. ADVANTAGE OF THE NONLINEAR COLLIMATOR FOR SUPERKEKB

A. Improved vertical instability threshold due to reduced impedance

Installing the NLC in the SuperKEKB LER has the most significant advantage of reducing the vertical impedance, which in turn increases the vertical instability threshold. As shown in Fig. 10, the measured threshold of the −1 mode instability of 1.25 mA at $\beta_y^* = 1$ mm before colllimator damage is already lower than the LER design bunch current (1.44 mA [29]). In the future operation of SuperKEKB, β_y^* will be further squeezed, and this threshold is expected to be even lower [7].

The impact of NLC on the vertical instability thresholds of TMCI and the −1 mode instability (denoted as Ib_{TMCI} and $Ib_{-1\,\mathrm{mode}}$, respectively) is demonstrated in Fig. 15. The vertical axis is the threshold current with and without the NLC and the horizontal axis is β_y^*. Here, it is assumed that Belle II tolerates the same amount of BG under the current operating conditions. Calculations involving the NLC were conducted under the assumption that D05V1 is used instead of D06V1. Impedance calculations focused solely on the vertical collimators and assumed a bunch length of 6 mm.

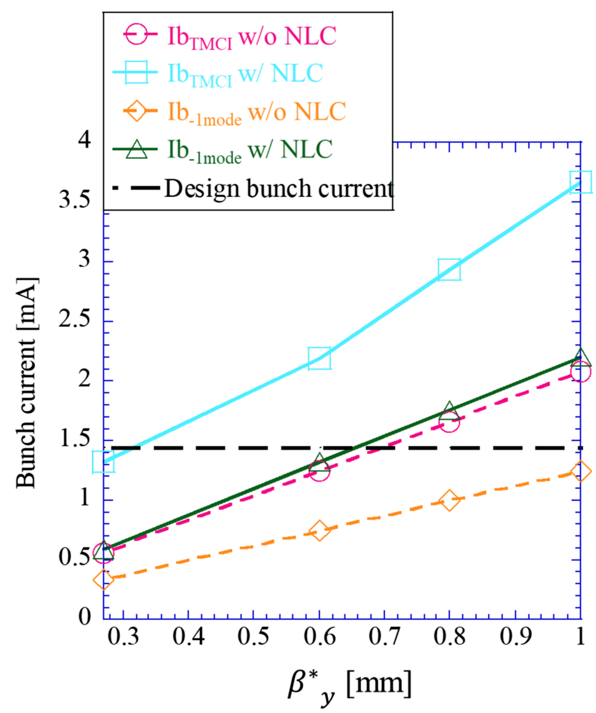

FIG. 15. The bunch current threshold at which the TMCI (Ib_{TMCI}) and vertical beam size blowup due to the −1 mode ($Ib_{-1\,\mathrm{mode}}$) occur versus β_y^*.

When β_y^* is squeezed, the vertical β function in the QCS increases, which increases the BG if the collimator half-gap is unchanged. To prevent this BG increase, the half-gap should be narrower when β_y^* is squeezed. The mechanism behind the vertical beam size blowup due to the–1 mode is not yet fully understood [19]. In this analysis, the threshold of the -1 mode was approximated based on the observed increase in beam size when the value of $\nu_y - (\nu_{y0} - \nu_s)$, as indicated by the orange arrow in Fig. 9, dropped below 0.009. $Ib_{-1\,\mathrm{mode}}$ is calculated as

$$Ib_{-1\,\mathrm{mode}} = (\nu_s - 0.009) / \sum k_{\perp,i} \beta_{y,i} / C_1 E/e. \quad (6)$$

The threshold of TMCI at $\beta_y^* = 1$ mm is estimated to be approximately 2.2 mA. Additionally, the recently discovered vertical mode coupling resulting from the interaction of the beam and the vertical impedance [22] suggests that the vertical impedance of the current SuperKEKB is too high to avoid beam-driven TMCI-like instability [21]. Further studies are necessary as this effect depends on the difference between the betatron tunes of the two beams.

It is evident that with the installation of the NLC, both Ib_{TMCI} and $Ib_{-1\,\mathrm{mode}}$ have improved. However, even with the NLC installed, the vertical instability threshold remains lower than the design current when the design β_y^* is reached. Therefore, further measures must be considered, such as improving the $\mathrm{B} \times \mathrm{B}$ feedback system.

B. Beam background reduction

Using NLC has the potential to reduce the BG level while keeping $\sum k_{\perp,i} \beta_{y,i}$ at the current level. Figure 16 shows the change of IR losses proportional to detector beam BG rates and beam lifetime when the half-gap of D05V1 is narrowed. The calculations were performed using the Monte-Carlo method discussed in Ref. [6], with the collimator settings listed in Table V. The Strategic Accelerator Design software [30], developed at the KEK Laboratory for multiturn particle tracking in circular colliders, was utilized to simulate beam losses and beam lifetime. It is important to note that the IR loss resulting from this calculation represents a single-beam BG source and does not include luminosity BGs. In Fig. 16, it is evident that the beam lifetime decreases when the D05V1 half-gap is smaller than 4 mm. Therefore, the collimator should be set to 4 mm or wider to avoid degradation of beam lifetime. Moreover, IR beam losses decreased when the half-gap was smaller than 20 mm. Table IV provides details of the calculation parameters used in the simulation.

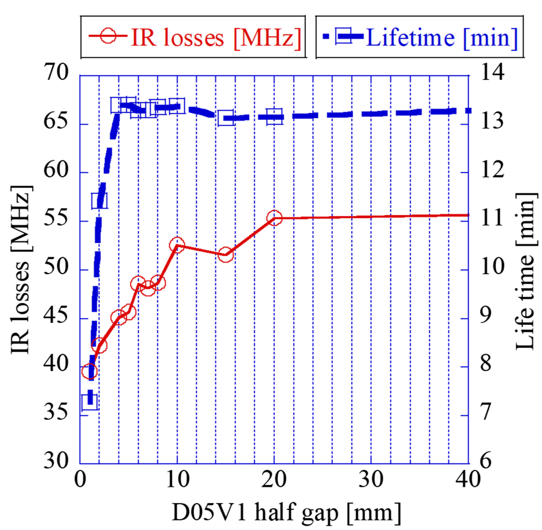

FIG. 16. Beam losses at the IR (±4 m from the IP) and beam lifetime versus the NLC aperture at $\beta_y^* = 1$ mm.

TABLE IV. Parameters of the beam tracking simulation to study the possible Belle II BG reduction using experimental collimator settings as on December 20, 2021.

Parameters	Units	Values in LER
Beam current	A	1.2
Number of bunches		1576
Horizontal emittance	nm	4.32
Vertical emittance	pm	43.2
Bunch length	mm	6

In addition to nonlinear collimation in both planes, as discussed above, the NLC can effectively clean the beam halo formed by particles scattered between D06V1 and the OHO section. This strengthens the motivation for implementing the NLC.

C. Sudden beam loss countermeasures with the nonlinear collimator

Here, we examine whether the NLC is effective to mitigate the SBL issue that caused several collimator damages during past operations.

The vertical beam size at the collimator (D05V1) is approximately expressed by the following equation:

$$\sigma_{yc} \cong R_{34} K_s \sigma_{ys} y_{\mathrm{center,s}}, \quad (7)$$

where σ_{yc} and σ_{ys} denote the vertical beam size at the collimator and SNAP.1, respectively, and the parameter $y_{\mathrm{center,s}}$ stands for the beam center position at SNAP.1. This expression is derived from the derivative of Eq. (4) with respect to y_s. The beam sizes at LER vertical collimators are compared in Table V. The vertical beam size of the D05V1 collimator is the value at which the bunch center has a vertical offset of 6.23 mm at the first SNAP. With this offset, the bunch center passes at the edge of the D05V1 jaw, and approximately half of the bunch charge hits the collimator, which occurs in the worst case of SBL events. As shown in this table, the vertical beam size at D05V1 is rather large compared to those at the other collimators

TABLE V. Transverse beam sizes at LER collimators at $\beta_y^* = 1$ mm.

Collimators	β_y (m)	σ_y (mm)	β_x (m)	η_x (m)	σ_x (mm)	$\sigma_x \times \sigma_y$ (mm^2)
D02V1	11.9	0.0226	26.2	0.378	0.439	0.00995
D06V2	20.6	0.0298	10.0	0.446	0.392	0.0117
D06V1	67.3	0.0539	14.6	0.516	0.459	0.0248
D05V1	4.05	0.178[a]	3.6	0.0	0.125	0.0222

[a] $y_{\mathrm{center,s}} = 6.23$ mm.

owing to nonlinear optics. However, the horizontal beam size at D05V1 is rather small compared to the other collimators because the horizontal β function at D05V1 is small and the horizontal dispersion is zero. Here, the energy spread of the beam is assumed to be at the design value of 7.42×10^{-4}. As a result, the cross section of the beam at D05V1 is not as large as that at D06V1, which was damaged several times owing to SBL events. We investigated whether it was possible to hit D05V1 with an abnormal beam during SBL and protect other critical components without damaging D05V1. This investigation showed that the beam size enlargement at D05V1 was not sufficient to protect it against collimator damage caused by the SBL.

Furthermore, we developed a new collimator jaw using a carbon fiber composite (CFC) as the collimator head material as a countermeasure to SBLs. This so-called Low-Z collimator with a collimator head length of 60 mm, which is expected to be robust against direct beam hits, was installed in the accelerator before the autumn 2020 operation. The low-Z collimator used as a spoiler had no negative effect on BG reduction [10]. With the low-Z collimator as the primary collimator in the ring with the narrowest aperture, accelerator operation was performed and an SBL event occurred. After inspection, it was confirmed that the low-Z collimator was undamaged. However, a beam-size blowup related to the impedance of the collimator occurred. Thus the low-Z collimator was replaced by a typical collimator with a short tantalum head, which has a smaller impedance. From this experience, we learned two things: first, light materials, such as CFC, are robust owing to the weak electromagnetic showers generated when the beam hits the collimator head; second, a long head causes the beam size to blowup, which interferes with the accelerator operation owing to the higher impedance.

Although the low-Z collimator failed, the head damage caused by the SBL is a serious issue; therefore, it must be addressed differently.

As an alternative, we considered the idea of using D06V1 upstream of the NLC as a spoiler collimator and the NLC as an absorber collimator. To use the D06V1 as a spoiler, it is necessary to install the collimator jaws with light material and with a short head length, and to narrow the aperture of D06V1. Hereafter, the method using NLC as an absorber collimator is abbreviated as MNAC (method using NLC as an absorber collimator). This two-stage collimation method is common in proton accelerators [31,32]. Additionally, the reason for setting D06V1 as the spoiler collimator is that the beam size at D06V1 is more than twice that at D06V2 (see Table V), which reduces damage to the head.

When MNAC is applied, the core of the beam passing through an abnormal orbit hits the spoiler collimator. However, because the spoiler collimator has a head made of light material and a short length, most of the particles pass through, and only the angle and energy of the particles change. Therefore, the beam core enlarges downstream of the spoiler. The enlarged abnormal beam then hits the NLC located downstream. The head of the NLC was not damaged because the NLC's head will not enlarge.

The D06V1 collimator, utilized as a spoiler, also serves as the primary collimator during the 2022 run, while the D05V1 collimator (NLC), used as an absorber, exhibits very low impedance, maintaining nearly the same level as at present even with MNAC implemented. The advantage of MNAC is that it reduces the probability of collimator head damage caused by the SBL without increasing the impedance from the present level. From the perspective of not damaging the collimator, it is desirable to use the lightest material possible for the spoiler collimator head; however, selecting a lighter material can lead to increased impedance due to the longer head length. Considering these factors, titanium, which has a low density and relatively high melting point, was selected.

We performed calculations to investigate whether the MNAC scenarios described above are valid. The calculations were performed for the following two types of simulations. Note that the calculations were performed assuming titanium as the head material for the spoiler collimator and tantalum as the head material for the absorber collimator. The optics file used in the simulation is $\beta_y^* = 1$ mm, and the half-gap of the collimator used for this simulation is shown in Table VI.

In the first type of calculation for MNAC, beam tracking simulations were performed to investigate whether particles scattered by hitting the spoiler collimator due to SBL were lost at IR. During the event when the D06V1 head was damaged, it was found that the beam orbit was offset by a maximum of -0.5 mm in the vertical direction at the point

TABLE VI. Horizontal and vertical collimator half-gap used for the simulation. Axis of the horizontal/vertical collimator was defined as + side for the ring outer/ceiling side. Jaws located the ring inner/floor side were denoted as In/Bottom and ring outer/ceiling side the ring as Out/Top. In the case of a horizontal/vertical collimator, β_x/β_y is shown. Phase advance with IP as 0 was defined (the decimal point is shown).

Collimators	β_x or β_y (m)	Half-gap of in/bottom (mm)	Half-gap of out/top (mm)	Phase advance (rad/π/2)
D06H1	24.2	−13.93	13.91	0.61
D06H3	24.2	−11.39	10.26	0.79
D03H1	29.0	−12.15	11.86	0.17
D02H1	20.8	−8.06	7.95	0.93
D02H2	36.5	−11.98	11.99	0.41
D02H3	50.8	−14.18	13.81	0.14
D02H4	20.4	−8.16	7.93	0.93
D06V1	67.3	−3.01	3.12	0.40
D06V2	20.6	−2.60	2.77	0.02
D05V1	4.05	−5.00	5.00	0.61
D02V1	11.9	−1.29	0.85	0.38

of the BOR (see Fig. 8), as discussed in the previous section. Therefore, we assumed that the damage to the head was caused by an offset of the beam orbit. However, simply offsetting the beam orbit by −0.5 mm in the vertical direction at the BOR position did not result in the beam hitting D06V1 at that turn. Therefore, we scanned the vertical angle to hit the D06V1 collimator under the condition that the beam was offset by −0.5 mm in the vertical direction at the BOR position. Calculations were performed using an optics file with $\beta_y^* = 1$ mm, as

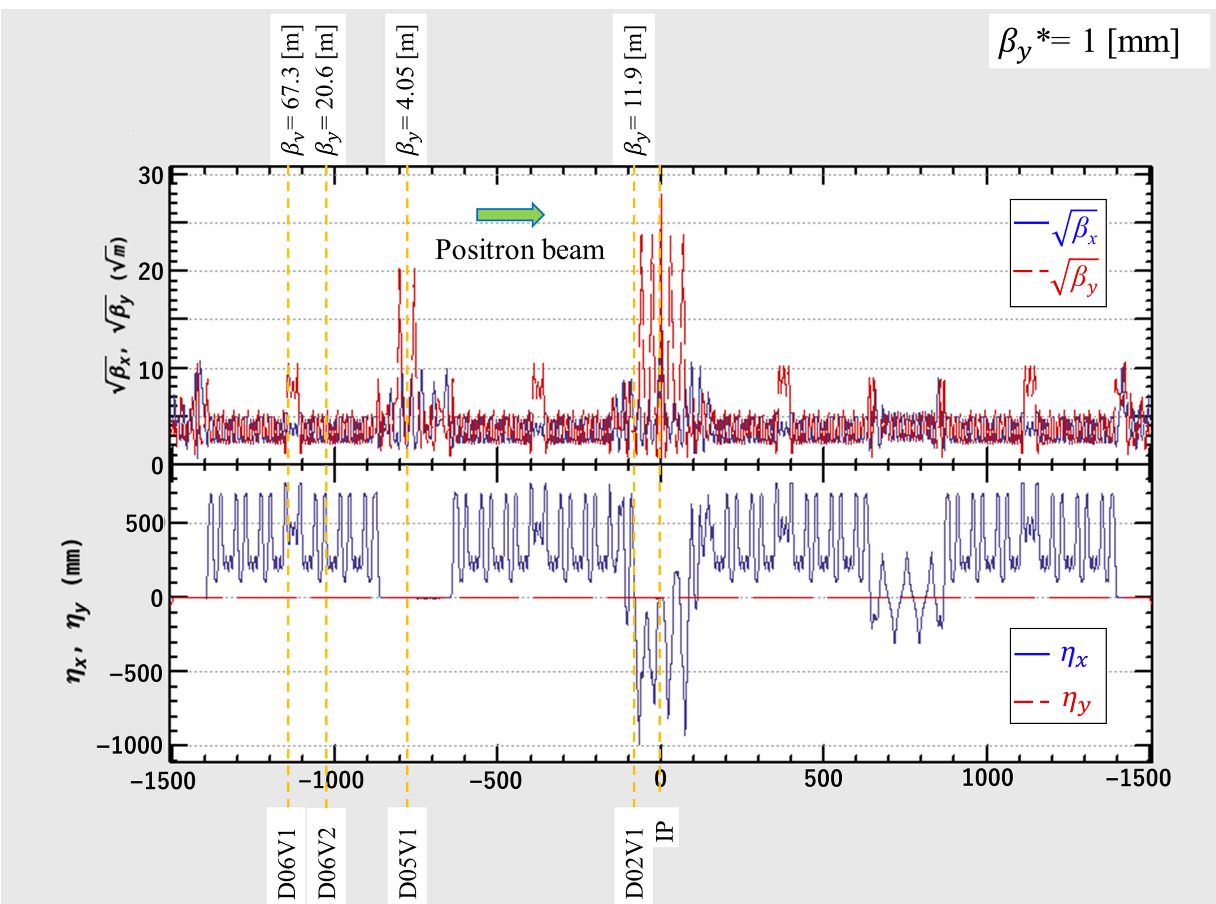

FIG. 17. Optics at $\beta_y^* = 1$ mm after the NLC installation.

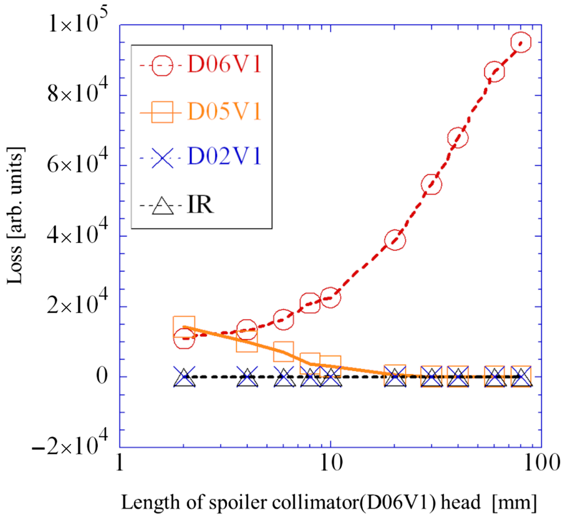

FIG. 18. Beam losses near each collimator (±4 m) versus length of the spoiler collimator (D06V1) head.

shown in Fig. 17. The results show that the particles kicked below −59 μrad and above 56 μrad, in the vertical direction, hit the D06V1 head. Figure 18 shows the result of beam tracking simulation with the beam orbit offset of −0.5 mm and kicked by 56 μrad in the vertical direction at the BOR position. The calculated collimator settings were used as on December 10, 2021. This figure shows the head length of the spoiler collimator on the horizontal axis and the loss near the relevant collimator (±4 m) plotted on the vertical axis. The results show that when the head length of the spoiler collimator (D06V1) is less than 10 mm, losses also occur near the absorber collimator (D05V1), but even with a head length of 2 mm, no losses appear in the IR. Therefore, it can be assumed that the MNAC does not produce IR losses in the IR. Moreover, from the calculations, it seems that there should not be any issue in using a spoiler collimator head length of less than 2 mm. However, because of fabrication problems and the risk of the electric field concentrated at the tip, as discussed in Ref. [10], 2 mm was set as the lower limit. We checked the MNAC setup only for the particular configuration in which the abnormal beam hits D06V1 first. The actual MNAC setup will be determined based on the beam conditions during the subsequent period of operation.

If the spoiler collimator and absorber collimator are damaged when the first SBL occurs, resulting in protrusions on the surface of the collimator head, this could cause an increase in the Belle II BG during accelerator operation after the collimator damage event. In the second type of calculation, beam irradiation simulations were performed using FLUKA [33,34]. A beam irradiation simulation was performed to ensure that the collimator head was designed to avoid damage, even when hit by beams with the highest possible current if MNAC was adopted. This particle simulation was performed using the results of the first-type

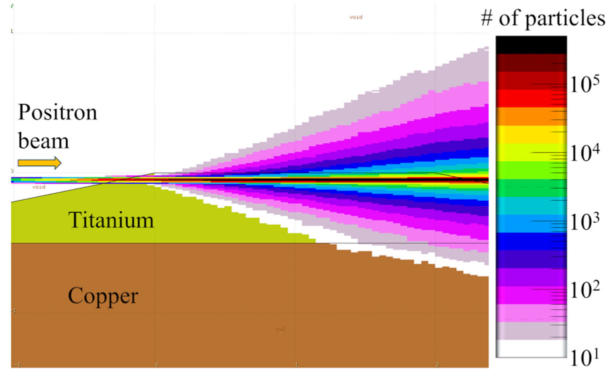

FIG. 19. The number of primary and secondary particles when the beam hits the D06V1 collimator.

calculation for MNAC. Figure 19 shows the number of particles when the positron beam hits the D06V1 used as a spoiler. This contour plot was calculated for a titanium head (head length of 2 mm) and a beam current of 1 mA. This indicates that the number of particles in the collimator increased due to the electromagnetic shower.

As candidate materials for collimator jaws, tantalum has a melting point of approximately 2900 K, and titanium melts at approximately 1500 K. Simulations were also performed to monitor the extent to which the volume of the collimator jaw exceeds the melting point and thus melts when high-current beams hit it. Figure 20 shows a simulation of the D06V1 as the spoiler collimator, with the beam current on the horizontal axis and the melting volume of the collimator jaw on the vertical axis. In the plot

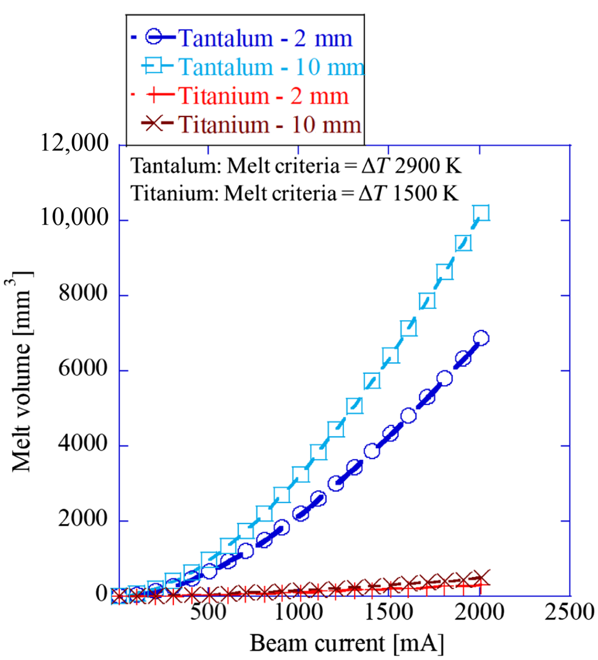

FIG. 20. Volume of tantalum and titanium (D06V1, spoiler) above its melting point versus the incident LER beam current.

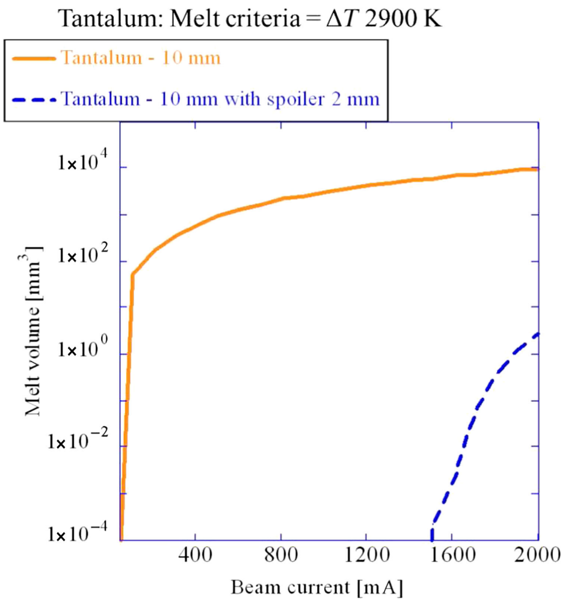

FIG. 21. Volume of tantalum (D05V1, absorber) above its melting point versus the incident LER beam current with/without a spoiler (D06V1).

in Fig. 20, a 100% beam loss appears to be assumed. For comparison, titanium and tantalum were also tested using simulations with varying jaw lengths. Although tantalum has a higher melting point, it has a larger melting volume at all currents, owing to its higher atomic number. In conclusion, titanium with a short length was preferred for D06V1 as a spoiler collimator.

For D05V1 as the absorber collimator, simulations are also performed to monitor the melting volume, as shown in Fig. 21, with the beam current on the horizontal axis and the melting volume on the vertical axis. A 10-mm long tatalum is chosen as the collimator jaw for effective absorption. Simulations are done with and without using D06V1 as a spoiler. For the spoiler collimator, the head material is titanium and a head length of 2 mm is assumed. The results indicate that, in the case of using a spoiler, the tantalum begins to melt when the lost beam current is over 1500 mA. Without spoiler, the tantalum begins to melt at approximately 50 mA due to the dense energy deposition. Therefore, we conclude that the two-stage MNAC scheme is effective in reducing the risk of damage to the collimator and the IR components due to the beam hitting. As described earlier, the causes of SBL are not yet well understood; therefore, MNAC will be adopted to ensure stable operation after LS1.

VI. POSSIBLE RISKS ASSOCIATED WITH THE NONLINEAR COLLIMATOR

NLC installation introduces a low-β section to the LER optics and potentially affects the dynamic aperture. Since part of the wiggler section is replaced by NLC, the total damping time will be approximately 10% longer, potentially impacting collective effects. In this section, we briefly address the possible risks associated with NLC.

A. Effect of the dynamic aperture decrease

The first risk associated with adopting NLC is a potential decrease in the dynamic aperture due to the requirement of an irregular lattice with very high vertical beta functions at the skew-sextupoles. A reduction in the dynamic aperture could impact not only the beam lifetime but also the injection efficiency. SuperKEKB utilizes off-axis betatron injection, and if the dynamic aperture is small, some of the injected beams may fall outside the dynamic aperture, leading to a decrease in injection efficiency. Concerns were raised regarding the potential reduction in injection efficiency due to the smaller dynamic aperture of the NLC. Therefore, a comparison of the dynamic apertures of the optics with and without NLC was conducted.

Figure 22 illustrates the results of the dynamic aperture calculation with a vertical-to-horizontal emittance ratio of 0.03, assuming an initial betatron oscillation phase of 0 (red) and $\pi/2$ (blue). This graph presents the dynamic

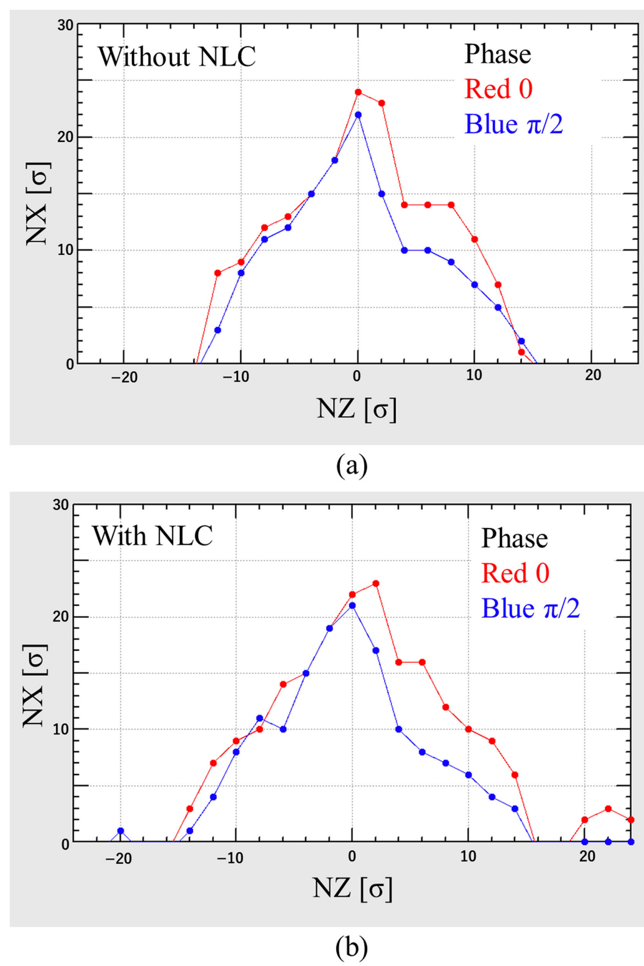

FIG. 22. Dynamic aperture (a) without and (b) with the NLC.

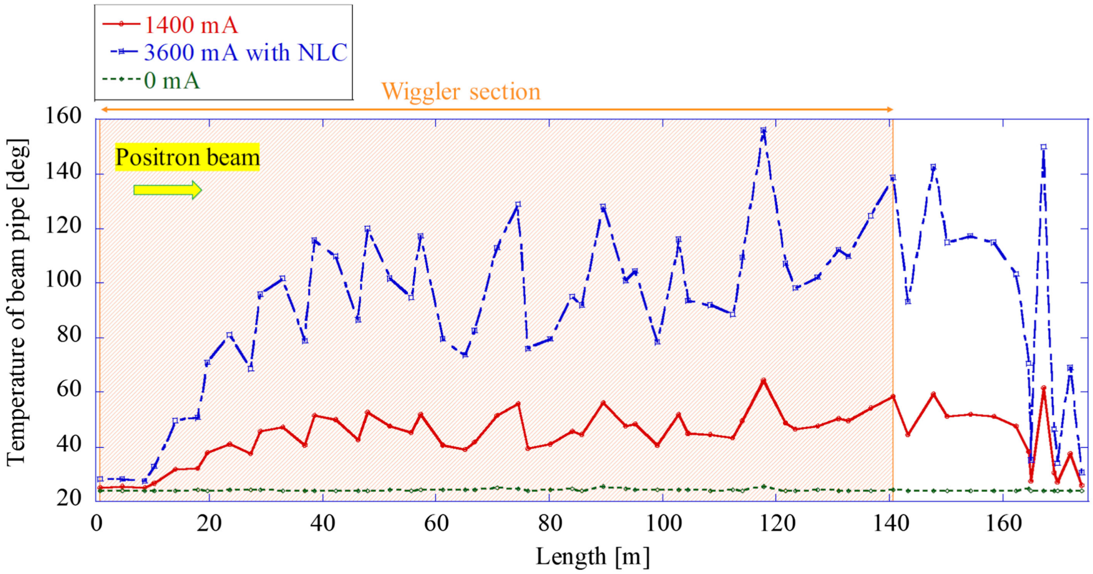

FIG. 23. Temperature of wiggler section measured at beam current of 1400 mA, assumed temperature of wiggler section at 3600 mA when magnetic field in wiggler section is increased to recover damping time.

aperture obtained from the calculation results of the tracking simulation, with the tracking starting point at the IP. The difference in dynamic apertures with and without the NLC was found to be negligible. Specifically, at a bunch current of 0.56 mA, simulations indicate Touschek lifetimes of 1273.9s with the NLC and 1404.6s without the NLC, with a difference of approximately 10%. Hence, the anticipated impact of NLC installation on beam lifetime and injection efficiency is minimal.

B. Partial disassembly of wiggler magnets

The longer radiation damping time resulting from the removal of the damping wigglers presents several potential risks. First, the reduced damping may lead to less effective suppression of the nonlinear effects of beam-beam interactions, potentially causing additional beam size blowup. Second, the damping of injected beam oscillations may decrease, potentially reducing injection efficiency and increasing background levels in the Belle II detectors. Despite these concerns, the expected reduction in damping time of approximately 10% is not anticipated to significantly impact machine performance. If necessary, measures such as increasing the magnetic field of other wiggler magnets can be implemented to restore the damping time. Additionally, adjustments to the horizontal dispersion in the "NIKKO" straight section can address changes in horizontal emittance resulting from the removal of the wiggler magnets, ensuring compatibility with the current lattice design. Furthermore, any alterations in the ring circumference due to the removal of the wiggler magnets can be compensated for using the chicane system located in the NIKKO section.

When the magnetic field of the remaining wiggler magnets was intensified to compensate for the longer radiation damping time, the beam pipe in the NIKKO wiggler section was exposed to strong SR. Figure 23 illustrates the temperatures of the beam pipe in the NIKKO wiggler section under different conditions. The red line represents the beam pipe temperature on the last day of the 2022ab run when the beam current reached 1400 mA, while the blue line indicates the assumed temperature under design current conditions with an increased magnetic field due to the NLC. The temperature of the beam pipe at zero current (green line) is also shown for reference. The blue value was calculated by assuming $1.3 \times (\text{temperature at } 1400 \text{ mA} - \text{temperature at } 0 \text{ mA}) \times 3600/1400$. Here, 1.3 is a coefficient of increase of the SR intensity accompanied by an intensification of the magnetic field to recover the damping time. From Fig. 23, it is assumed that the maximum temperature is above 150 °C. Such elevated temperatures pose an increased risk of stress on the flange and potential vacuum leakage. To mitigate this risk, the decision was made to augment the number of SR masks and cooling fans, thereby reducing the likelihood of vacuum leaks.

VII. SUMMARY

This paper addresses three primary challenges concerning the SuperKEKB LER collimators: (i) detector beam background, (ii) beam instability, and (iii) durable collimator system to countermeasure sudden beam loss events during present and future beam operations.

The TOP counter within the Belle-II detector is particularly susceptible to beam background. Extrapolating current beam conditions with $\beta_y^* = 1$ mm optics suggests that the beam background level will approach the TOP counter's limit at approximately 1.6A. To accommodate higher

LER beam currents or further squeezing of β_y^*, narrower gap apertures in the vertical collimators will be required. However, a challenge to implementing narrower collimator apertures is the potential increase in impedance, which could lead to beam instability. The adoption of NLC is proposed as a solution to significantly reduce impedance and mitigate instability issues.

A detailed estimation of the threshold of instabilities was performed as the function of the IP vertical beta function (β_y^*) in LER. There are two types of problematic beam instability: the "-1 mode instability" and TMCI. The -1 mode instability was discovered in SuperKEKB LER as the vertical beam size blowup and has been studied in detail during the machine study on whether NLC is required at SuperKEKB. This instability is caused by interplay between impedance and the bunch-by-bunch feedback. Another significant instability in the SuperKEKB LER is TMCI. At the current β_y^* of 1 mm, the threshold bunch current for the–1 mode instability is 1.25 mA, lower than the designed value of 1.44 mA. However, using the NLC (D05V1) instead of the current D06V1 collimator is estimated to increase the instability threshold to approximately 2.1 mA. Yet, with a lower β_y^* of approximately 0.7 mm, the estimated threshold bunch current decreases to the design value even with the NLC.

The threshold bunch current for TMCI at the current β_y^* of 1 mm is estimated to be approximately 2.2 mA. However, the newly discovered effect on beam-beam mode coupling suggests that the TMCI threshold may decrease significantly due to beam-beam interaction, depending on the betatron tune difference between the two beams. Further investigation is required to understand this effect fully.

Moreover, it is important to note that setting a narrower collimator aperture to reduce beam background in the TOP counter may lower the instability threshold in the future.

Sudden beam loss poses a significant challenge to SuperKEKB performance. To address this issue, we propose the use of a spoiler collimator with low Z and short jaws, alongside an NLC as an absorber collimator. This strategy aims to prevent damage even during sudden beam loss events. Notably, this approach maintains collimator impedance similar to the current scheme, offering an interim solution until the root cause of such events is identified and resolved permanently.

The implementation of NLC in the SuperKEKB LER is motivated by its effectiveness in addressing the major challenges associated with collimators. Installation of NLC was completed by the end of 2023, and its operational effectiveness will be assessed through beam studies in 2024.

Furthermore, potential side effects of NLC installation are discussed. The first concern is a potential decrease in dynamic aperture due to the irregular lattice with high vertical beta functions in the NLC section. However, simulations suggest minimal impact, which will be verified through beam studies in 2024. The second concern is the longer radiation damping time resulting from partial disassembly of wiggler magnets for NLC installation, potentially affecting beam-beam performance and injection efficiency. These effects will also be thoroughly investigated during the 2024 beam operation. If beam performance is compromised, we plan to restore radiation damping time by intensifying the strength of the remaining wiggler magnets.

ACKNOWLEDGMENTS

The authors thank the SuperKEKB and Belle II members for their constant support of our work.

[1] Z. Doležal and S. Uno, Belle II Technical Design, Report No. KEK-2010-1, 2010, https://www-superkekb.kek.jp/documents/B2TDR.pdf.

[2] Y. Ohnishi *et al.*, Accelerator design at SuperKEKB, Prog. Theor. Exp. Phys. **2013**, 03A011 (2013).

[3] N. Ohuchi *et al.*, Superkekb beam final focus superconducting magnet system, Nucl. Instrum. Methods Phys. Res., Sect. A **1021**, 165930 (2022).

[4] A. Natochii, T. Browder, L. Cao, K. Kojima, D. Liventsev, F. Meier, K. Nakamura, H. Nakayama, C. Niebuhr, A. Novosel *et al.*, Beam background expectations for Belle II at SuperKEKB, arXiv:2203.05731.

[5] T. Ishibashi, S. Terui, Y. Suetsugu, K. Watanabe, and M. Shirai, Movable collimator system for SuperKEKB, Phys. Rev. Accel. Beams **23**, 053501 (2020).

[6] A. Natochii, S. E. Vahsen, H. Nakayama, T. Ishibashi, and S. Terui, Improved simulation of beam backgrounds and collimation at SuperKEKB, Phys. Rev. Accel. Beams **24**, 081001 (2021).

[7] T. Ishibashi, M. Migliorati, D. Zhou, K. Shibata, T. Abe, M. Tobiyama, Y. Suetsugu, and S. Terui, Impedance modelling and single-bunch collective instability simulations for the SuperKEKB main ring, to be published.

[8] A. W. Chao, M. Tigner, H. Weise, and F. Zimmermann, *Handbook of Accelerator Physics and Engineering* (World Scientific, Singapore, 2023).

[9] H. Nakayama, K.-I. Kanazawa, Y. Suetsugu, Y. Ohnishi, Y. Funakoshi, K. Ohmi, and D. Zou, Small-beta collimation at SuperKEKB to stop beam-gas scattered particles and to avoid transverse mode coupling instability, Conf. Proc. C **1205201**, 1104 (2012).

[10] S. Terui, T. Ishibashi, T. Abe, Y. Funakoshi, H. Nakayama, K. Ohmi, D. Zhou, A. Natochii, and N. Yoshifuji, Low-z collimator for SuperKEKB, Nucl. Instrum. Methods Phys. Res., Sect. A **1047**, 167857 (2023).

[11] K. Kanazawa, 21st KEKB Accelerator Review, 2016, https://www-kekb.kek.jp/MAC/2016/Report/Kanazawa.pdf.

[12] H. Nakayama, Summary of beam background in 2020c, MDI taskforce meeting (2021), https://kds.kek.jp/event/36729/.

[13] A. Natochii *et al.*, Measured and projected beam backgrounds in the Belle II experiment at the SuperKEKB collider, Nucl. Instrum. Methods Phys. Res., Sect. A **1055**, 168550 (2023).

[14] Y. Horii (Belle-II PID), Top detector for particle identification at the Belle II experiment, Proc. Sci. EPS-HEP2013 (2013) 500.

[15] S. Terui, Y. Funakoshi, H. Hisamatsu, T. Ishibashi, K. Kanazawa, Y. Ohnishi, K. Shibata, M. Shirai, Y. Suetsugu, and M. Tobiyama, Report on collimator damaged event in SuperKEKB, in *Proceedings of the 12th International Particle Accelerator Conference, IPAC-2021, Campinas, Brazil* (JACoW, Geneva, Switzerland, 2021), WEPAB359.

[16] M. Tobiyama and J. W. Flanagan, Development of bunch current and oscillation recorder for SuperKEKB accelerator, in *Proceedings of the 1st International Beam Instrumentation Conference, IBIC-2012, Tsukuba, Japan* (JACoW, Geneva, Switzerland, 2012).

[17] H. Ikeda, T. Abe, M. Aversano, H. Fukuma, Y. Funakoshi, T. Ishibashi, H. Kaji, T. Koga, Y. Liu, H. Nakayama, G. Mitsuka, S. Terui, M. Tobiyama, Y. Suetsugu, and K. Yoshihara, Observation of sudden beam loss in SuperKEKB, in *Proceedings of the 14th International Particle Accelerator Conference, IPAC-2023, Venice, Italy* (JACoW, Geneva, Switzerland, 2023), p. 716.

[18] S. Terui, H. Fukuma, Y. Funakoshi, T. Ishibashi, T. Nakamura, K. Ohmi, Y. Ohnishi, M. Tobiyama, and R. Ueki, The report of machine studies related to the vertical beam size blow-up in SuperKEKB LER, in *Proceedings of the 13th International Particle Accelerator Conference, IPAC-2022, Bangkok, Thailand* (JACoW, Geneva, Switzerland, 2022), WEPOTK050.

[19] K. Ohmi, H. Fukuma, T. Ishibashi, S. Terui, M. Tobiyama, and D. Zhou, Study for -1 mode instability in SuperKEKB low energy ring, in *Proceedings of the 65th ICFA Advanced Beam Dynamics Workshop on High Luminosity Circular e^+e^- Colliders, eeFACT2022, Frascati, Italy* (JACoW, Geneva, Switzerland 2023), p. 119.

[20] E. Mulyani, J. W. Flanagan, M. Tobiyama, H. Fukuma, H. Ikeda, and G. Mitsuka, First measurements of the vertical beam size with an x-ray beam size monitor in superkekb rings, Nucl. Instrum. Methods Phys. Res., Sect. A **919**, 1 (2019).

[21] Y. Zhang, N. Wang, K. Ohmi, D. Zhou, T. Ishibashi, and C. Lin, Combined phenomenon of transverse impedance and beam-beam interaction with large Piwinski angle, Phys. Rev. Accel. Beams **26**, 064401 (2023).

[22] K. Ohmi, Y. Zhang, and C. Lin, Beam-beam mode coupling in collision with a crossing angle, Phys. Rev. Accel. Beams **26**, 111001 (2023).

[23] JLC-I, KEK, Technical Report No. KEK-92-16, 1992, Sec. IV.2.4, https://libextopc.kek.jp/preprints/PDF/1992/9224/9224016.pdf.

[24] N. Merminga, J. Irwin, R. Helm, and D. Ruth, R, Collimation system for a TEV linear collider, Part. Accel. **48**, 85 (1994).

[25] N. Toge, Jlc design study, Technical Report No. KEK-97-1, 1997.

[26] A. Faus-Golfe and F. Zimmermann, A Nonlinear collimation system for CLIC, in *Proceedings of the 8th European Particle Accelerator Conference, Paris, 2002* (EPS-IGA and CERN, Geneva, 2002), pp. 533–535.

[27] J. Resta Lopez, R. Assmann, S. Redaelli, G. Robert-Demolaize, D. Schulte, F. Zimmermann, and A. Faus-Golfe, An alternative nonlinear collimation system for the LHC, Conf. Proc. C **060626**, 246 (2006).

[28] J. Resta Lopez, F.-G. Angeles, L. Lari, and F. Zimmermann, Update on nonlinear collimation scheme for the LHC, in *Proceedings of 5th International Particle Accelerator Conference, IPAC-2014, Dresden, Germany* (JACoW, Geneva, Switzerland, 2014), p. 151.

[29] SuperKEKB design report, https://kds.kek.jp/event/15914/.

[30] Strategic accelerator design, https://acc-physics.kek.jp/SAD/.

[31] R. Assmann *et al.*, The final collimation system for the LHC, Conf. Proc. C **060626**, 986 (2006).

[32] R. Bruce *et al.*, Simulations and measurements of beam loss patterns at the CERN large hadron collider, Phys. Rev. ST Accel. Beams **17**, 081004 (2014).

[33] C. Ahdida, D. Bozzato, D. Calzolari, F. Cerutti, N. Charitonidis, A. Cimmino, A. Coronetti, G. D'Alessandro, A. Donadon Servelle, L. Esposito, R. Froeschl, R. Alia, A. Gerbershagen, S. Gilardoni, D. Horváth, G. Hugo, A. Infantino, V. Kouskoura, A. Lechner, and M. Widorski, New capabilities of the FLUKA multi-purpose code, Front. Phys. **9**, 788253 (2022).

[34] G. Battistoni *et al.*, Overview of the FLUKA code, Ann. Nucl. Energy **82**, 10 (2015).